Proceedings of the ASME 2018 Dynamic Systems and Control Conference
DSCC2018
September 30-October 3, 2018, Atlanta, Georgia, USA

SAND2018-6930C

DSCC2018-9141

ENERGY IMPLICATIONS OF TORQUE FEEDBACK CONTROL AND SERIES ELASTIC ACTUATORS FOR MOBILE ROBOTS

Stephen P. Buerger
Sandia National Laboratories
Albuquerque, NM, USA

Anirban Mazumdar
Georgia Institute of Technology
Atlanta, GA, USA

Steven J. Spencer
Sandia National Laboratories
Albuquerque, NM, USA

ABSTRACT

Torque feedback control and series elastic actuators are widely used to enable compact, highly-geared electric motors to provide low and controllable mechanical impedance. While these approaches provide certain benefits for control, their impact on system energy consumption is not widely understood. This paper presents a model for examining the energy consumption of drivetrains implementing various target dynamic behaviors in the presence of gear reductions and torque feedback. Analysis of this model reveals that under cyclical motions for many conditions, increasing the gear ratio results in greater energy loss. A similar model is presented for series elastic actuators and used to determine the energy consequences of various spring stiffness values. Both models enable the computation and optimization of power based on specific hardware manifestations, and illustrate how energy consumption sometimes defies conventional best-practices. Results of evaluating these two topologies as part of a drivetrain design optimization for two energy-efficient electrically driven humanoids are summarized. The model presented enables robot designers to predict the energy consequences of gearing and series elasticity for future robot designs, helping to avoid substantial energy sinks that may be inadvertently introduced if these issues are not properly analyzed.

INTRODUCTION

Torque feedback control and series elastic actuators (SEAs), used together or independently, are popular strategies for facilitating physical interaction using high-impedance actuators (e.g. servo-hydraulic or highly-geared electromagnetic). In torque feedback control, the output torque (or force) is measured at or near the point of interaction with the environment, and used as part of a feedback control scheme to regulate either the torque output [1], or the relationship between torque and motion at the point of interaction (the mechanical impedance) [2]. By feeding back the output torque, a drivetrain (actuator and transmission) with high intrinsic impedance (large friction and reflected inertia) may be made to appear to have low impedance. SEA's use an elastic element in series between a drivetrain and the environment. The elastic element allows a position-controlled actuator to effectively control output torque by servo-controlling spring deflection, while also mitigating impact shock [3]. Both approaches are theoretically compatible with large gear ratios, meaning that large torques may be drawn from compact motors.

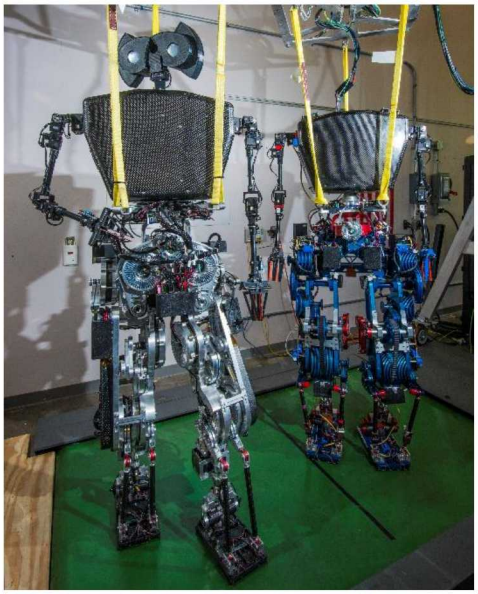

FIGURE 1. WANDERER (L) AND STEPPR (R) ENERGY-EFFICIENT HUMANOID ROBOTS.

The use of these approaches stems from the need to render controllable impedance or directly control torque to enable interactions between a robotic system and an environment. Common applications include physically-interactive manipulation (e.g. exoskeletal and rehabilitative devices,

Sandia National Laboratories is a multimission laboratory managed and operated by National Technology & Engineering Solutions of Sandia, LLC, a wholly owned subsidiary of Honeywell International Inc., for the U.S. Department of Energy's National Nuclear Security Administration under contract DE-NA0003525.

prosthetics, and assembly robots) and dynamic legged locomotion. In these manipulation tasks (e.g. see [4-6]), there is frequently a need to render highly variable virtual environments, e.g. virtual walls that require both near-zero impedance and very stiff behavior. For legged robots, torque or impedance control is generally needed to implement reactive walking schemes, manage ground contact transitions, and perform behaviors that are not strictly trajectory-based such as walking robustly over small unmodeled obstacles. A number of recent humanoid bipeds use SEA's [7-9].

A well-known drawback of torque feedback is that it can induce coupled instability, particularly when in contact with stiff environments [10]. The instability stems from attempting to reduce the apparent inertia below the level of the actual physical system by using a non-collocated actuator and torque sensor, and is independent of the details of the control implementation. Natural admittance control (NAC) allows friction to be suppressed while mitigating instability by ensuring that the full inertia of the physical system is felt at the point of interaction [11]. This, however, limits the torque control quality; pure torque control requires zero impedance (zero inertia and friction).

SEA's usually incorporate a torque feedback scheme, and can improve coupled stability by effectively limiting the stiffness of the interaction with the environment to that of the elastic element. This is particularly effective if damping across the elastic element is tailored appropriately to absorb the energy that might destabilize interaction [12]. A clear disadvantage is reduced high-frequency bandwidth. Sometimes cited (e.g. see [3]), but seldom explored in depth (outside of particular applications such as hopping), is the potential for compliant SEA elements to save net energy by advantageously storing and releasing energy during robot behaviors. For mobile robots in particular (and especially legged robots, which are generally very inefficient), energy efficiency is very important as it translates into mission duration and range.

In this paper we analyze the energy implications of using high-impedance drivetrains with torque feedback and SEA's. We identify the conditions under which these approaches save and cost energy. We focus on the energy impact of compensating for increased gear reductions (which enable the use of smaller motors) with feedback, and of tailoring SEA stiffness for different target behaviors. This analysis reveals that these approaches sometimes come with a substantial energy penalty. Therefore, mobile robot designers should carefully consider energy issues when considering these drivetrain architectures. Previous works have assessed the energetic impact of series elasticity by comparing it with parallel elastic elements [13-17]. A primary outcome is that series elastic actuators can save energy, but the savings are narrowly focused within specific operating frequency or speed bounds [13-15]. Prior experimental work has demonstrated that electrical power consumption can increase dramatically when operating beyond the passive SEA bandwidth [9]. Other relevant work has focused on examining the role of physical models on predictions for geared electric motor consumption [18] and the optimization of motor and gearing parameters for a specific task based on energy and bandwidth [19]. The role that torque feedback control and the tailoring of motor size and gear ratio play in determining energy consumption remains unclear. Clarifying this is the goal of the work presented herein.

In this paper we analyze a model for torque feedback control and consider the energy implications of using feedback to compensate for differences between the intrinsic physical system impedance and the desired endpoint behavior. Subsequently we include series elastic components and evaluate the impact of spring stiffness on energy consumption. We summarize relevant results of design optimizations for energy efficient legged humanoid robots (Fig. 1) in which the energy impact of series elasticity is explored for a variety of robot leg trajectories. Finally, we provide discussion and conclusions.

NOMENCLATURE

B_G	Rotational damping coefficient, gear output (*Nms/rad*)
B_M	Rotational damping coefficient, motor (*Nms/rad*)
B_O	Rotational damping coefficient, output link (*Nms/rad*)
B_T	Total drivetrain rot. damping coefficient (*Nms/rad*)
c	*cos ωt*
h	Motor coil height (*m*)
I_M	Motor current (*A*)
J_D	Desired control moment of inertia (Nms^2/rad)
J_G	Moment of inertia, gear output (Nms^2/rad)
J_M	Moment of inertia, motor (Nms^2/rad)
J_O	Moment of inertia, output link (Nms^2/rad)
J_T	Total drivetrain moment of inertia (Nms^2/rad)
K_D	Desired control stiffness (*Nm/rad*)
K_m	Motor constant ($Nm/\sqrt{W}$)
K_S	Series elastic element coefficient (*Nm/rad*)
K_t	Motor torque constant (*Nm/A*)
N	Gear reduction ratio
ω	Frequency of cyclic motion (*rad/s*)
P_M	Power applied to motor (*W*)
R_M	Motor resistance (Ω)
σ	Laplace variable
s	*sin ωt*
τ_M	Motor torque (*Nm*)
τ_O	Applied load torque at output (*Nm*)
θ	Rotation angle (*rad*)
$\dot{\theta}$	Angular velocity (*rad/s*)
$\ddot{\theta}$	Angular acceleration (rad/s^2)
θ_G	Rotation angle of gear output stage (*rad*)
$\dot{\theta}_G$	Angular velocity of gear output stage (*rad/s*)
$\ddot{\theta}_G$	Angular acceleration of gear output stage (rad/s^2)
θ_O	Rotation angle of output link (*rad*)
$\dot{\theta}_O$	Angular velocity of output link (*rad/s*)
$\ddot{\theta}_O$	Angular acceleration of output link (rad/s^2)
w	Motor coil width (*m*)

ENERGY ANALYSIS OF TORQUE FEEDBACK CONTROL

In this section we develop and analyze a model for energy consumption for geared electric motor-based drivetrains that use endpoint torque feedback. This energy-focused model enables analytical and rapid evaluation of the interplay between increasing the gear ratio (generally done to enable the use of lower-torque, smaller / lighter motors) and the energy expended using torque feedback to achieve desired endpoint behavior.

Power Consumption Model

The model, shown in Fig. 2, includes a rotary motor driving an output stage link through a gear reduction with ratio N. Output torque τ_O is applied to the geared output, which has inertia J_G and linear rotational damping coefficient B_G. The motor has inertia J_M, damping B_M, resistance R_M, torque constant K_t, motor constant K_m, and produces torque τ_M via current I_M. Transmission backlash, while important for control, does not fundamentally affect energy consumption and is ignored.

The mechanical dynamics in the link frame are:

$$J_T\ddot{\theta} + B_T\dot{\theta} = N\tau_M + \tau_O \tag{1}$$

where the total apparent inertia and damping at the output are:

$$J_T = J_G + N^2 J_M \quad \text{and} \quad B_T = B_G + N^2 B_M \tag{2}$$

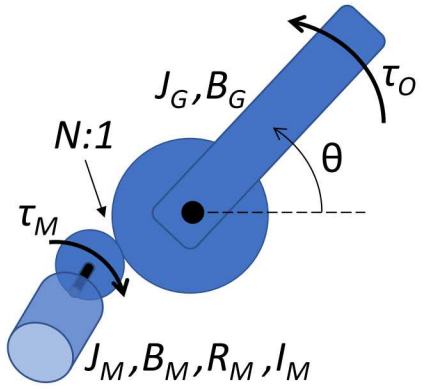

FIGURE 2. MODEL OF RIGID ROTARY LINK DRIVEN BY GEARED ROTARY MOTOR.

To achieve an arbitrary output torque τ_O, regardless of control implementation, τ_M must approach the following:

$$\tau_M = \frac{J_T}{N}\ddot{\theta} + \frac{B_T}{N}\dot{\theta} - \frac{\tau_O}{N} \tag{3}$$

A simple electromechanical model for the motor is:

$$\tau_M = K_t I_M; \qquad K_m = K_t/\sqrt{R_M} \tag{4}$$

The power to the motor includes joule heating (I^2R) losses as well as the mechanical output:

$$P_M = I_M^2 R_M + N\tau_M\dot{\theta} \tag{5}$$

Substituting (1), (3), and (4) into (5) produces:

$$P_M = \left(\frac{J_T}{K_m N}\ddot{\theta} + \frac{B_T}{K_m N}\dot{\theta} - \frac{\tau_O}{K_m N}\right)^2 + \left(J_T\ddot{\theta} + B_T\dot{\theta} - \tau_O\right)\dot{\theta} \tag{6}$$

Substituting (2) and rearranging produces:

$$P_M = \left[\frac{N}{K_m}\left(J_M\ddot{\theta} + B_M\dot{\theta}\right) + \frac{1}{K_m N}\left(J_G\ddot{\theta} + B_G\dot{\theta} - \tau_O\right)\right]^2 + \left[J_G\ddot{\theta} + B_G\dot{\theta} + N^2\left(J_M\ddot{\theta} + B_M\dot{\theta}\right) - \tau_O\right]\dot{\theta} \tag{7}$$

Equation (7) is a general expression for motor power, regardless of output behavior. The first bracketed term represents the I^2R losses that result from the production of torque via current; the first interior term represents power spent overcoming motor dynamics, and the second is power to overcome link dynamics and produce the desired output. The second bracketed term is the mechanical power, which similarly includes elements to move the motor, the link, and produce output torque.

Scaling with Gear Ratio and Motor Size

Aggressive gearing is frequently used in robotics to increase the torque output from smaller motors. In the model in Fig. 2, we are interested in the effect of increasing N, simultaneously shrinking the motor to achieve a specified maximum output torque, and then closing a feedback control loop around output torque to achieve the desired output. To analyze this requires a model of how electric motor parameters scale with the motor's output torque capacity. One simplified way to model this is to consider a rotary motor with windings contained in a cylinder of height h. The individual windings are approximately rectangular with width w, as shown in Fig. 3. If other aspects of the motor design are kept constant, and any torque generated by the winding end turns is neglected, the motor torque capacity (and K_t) may be considered proportional to h. J_M and B_M may also be approximated as proportional to h. Because the wire coils change in length with h but not in their width, R_M changes with h in a way that depends on motor geometry. If the width of the coils is neglected, then the total wire length increases in proportion to h, and R_M is proportional to h. In actuality, R_M scales more weakly with h. For the analysis that follows, we assume that R_M changes proportionally with h, which means that K_m is proportional to $h^{0.5}$. This assumption is most energetically favorable to the common approach of using aggressive gear reductions and small motors; if R_M is more weakly dependent on h, then K_m scales more strongly with h, and the results that follow become less favorable to gearing. For specific design cases, the relationships between motor parameters may be derived from actual candidate motors.

When N is varied around an operating point, the motor torque capacity required to execute a behavior (and therefore h, J_M, and B_M) may be scaled in inverse proportion, while K_m scales with $N^{-0.5}$. So with respect to the terms in (7), the following proportionality relationships may be defined:

$$N^2 J_M \sim N^2 B_M \sim N; \quad \frac{N}{K_m} J_M \sim \frac{N}{K_m} B_M \sim K_m N \sim \sqrt{N} \tag{8}$$

Increasing gear ratio N, and simultaneously reducing motor size can either increase or decrease required energy. This depends on the motion profile, loading, and system parameters. Considering several common control cases can provide additional insight, particularly for the (highly relevant) case when trajectories are cyclical.

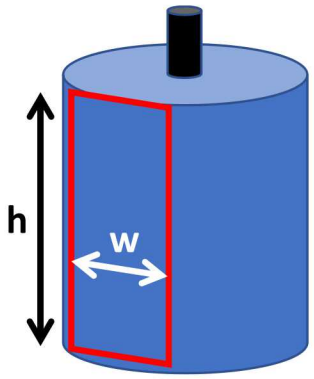

FIGURE 3. MODEL OF MOTOR WINDING GEOMETRY. A SINGLE REPRESENTATIVE COIL IS HIGHLIGHTED IN RED.

Control Cases of Interest

Several generic examples that cover a broad spectrum of typical desired actuator behaviors are examined in this section. Desired inertial and stiffness actuator dynamics are considered. These cases choose impedance-based actuator behaviors, which enables actuator analysis and control to be decoupled from the load dynamics. Load dynamics may be difficult to predict for legged robots and may vary widely during a gait cycle. Pure torque control, which includes a wide variety of actuator behavior that is controlled independent of the load, is also analyzed. In this analysis we make no assumptions about the load dynamics – we rely only on an assumption of cyclic motion, which is valid for any sustained walking behaviors.

Inertial Control One common behavior is to mimic a desired inertia J_D. For example, the use of NAC might seek to target $J_D<J_T$, i.e. to present an apparent drivetrain inertia to the load that is less than the physical value [11]. Conversely, $J_D>J_T$ may be used to provide loading for intelligent rehabilitation devices. An inertia impedance controller takes the form:

$$\tau_O = J_D \ddot{\theta} \tag{9}$$

Substituting into (7) produces:

$$P_M = \left[\frac{(N^2 J_M + J_G - J_D)}{K_m N}\ddot{\theta} + \frac{(N^2 B_M + B_G)}{K_m N}\dot{\theta}\right]^2 + (N^2 J_M + J_G - J_D)\ddot{\theta}\dot{\theta} + (N^2 B_M + B_G)\dot{\theta}^2 \tag{10}$$

Further insights may be gained by exploring cyclical behaviors in the frequency domain. Cyclical behaviors are typical for many relevant applications, including gaits for legged robots and exoskeletons as well as repetitive manipulation tasks. Without loss of generality, cyclical behavior may be analyzed by assuming the link moves in a sinusoidal manner; similar results are obtained for arbitrary cyclic trajectories by approximating with a Fourier series. Sinusoidal behavior may be analyzed by substituting $\theta = \sin \omega t$ and its derivatives. In the equations that follow, $s = \sin \omega t$ and $c = \cos \omega t$. Substituting into (10) produces:

$$P_M = \left[-\left(\frac{N^2 J_M + J_G - J_D}{K_m N}\right)\omega^2 s + \left(\frac{N^2 B_M + B_G}{K_m N}\right)\omega c\right]^2 - (N^2 J_M + J_G - J_D)\omega^3 sc + (N^2 B_M + B_G)\omega^2 c^2 \tag{11}$$

Integrating this expression over the interval $t = 0: 2\pi/\omega$ yields energy for a full period. Dividing by that period provides the average power. Because the integral of ($sin \cdot cos$) over an integer period is zero, the third term (mechanical power due to inertia) disappears. Physically, this is because no net energy is required to oscillate a free mass. The cross term from squaring the bracketed quantity also disappears. The resulting average motor power is:

$$P_{avg} = \frac{1}{2}\left(\frac{N^2 J_M + J_G - J_D}{K_m N}\right)^2 \omega^4 + \frac{1}{2}\left(\frac{N^2 B_M + B_G}{K_m N}\right)^2 \omega^2 + \frac{1}{2}(N^2 B_M + B_G)\omega^2 \tag{12}$$

Examination of this expression produces several important insights. The third term (mechanical power due to friction) increases with N at all frequencies. The first two terms relate to the I^2R loss due to the difference between the physical and desired inertia and damping, respectively. These two terms increase with N for all ω as long as: 1) $J_D<J_T$, and 2) the link inertia and damping do not dominate the reflected motor dynamics. The latter is true for most geared robot designs.

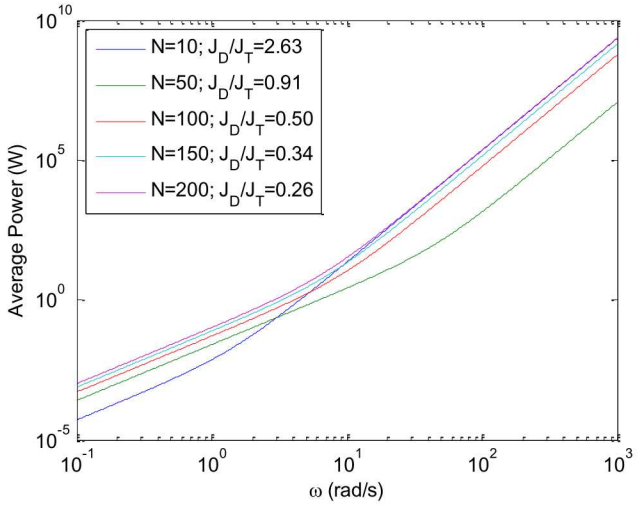

FIGURE 4. AVERAGE POWER VERSUS FREQUENCY FOR TORQUE FEEDBACK MODEL WITH DESIRED INERTIA. GEAR RATIO *N* AND RATIO OF DESIRED / PHYSICAL INERTIAS ARE SHOWN.

Thus, when torque feedback is used to reduce the apparent inertia in the presence of significant gearing, it usually requires more energy to use a larger gear ratio and smaller motor. In addition, if friction is eliminated from the physical system, the last two terms in (12) disappear, but the first remains. This makes clear that friction is not the sole source of loss in torque feedback systems; compensating for undesired inertia is a large potential loss. The power lost can grow quite large when feedback is aggressively used to reduce inertia. Figure 4 plots the expression in (12) for several different gear ratios. The motor parameters are based on a Maxon 167131 motor for $N=100$, and are scaled according to (8) for other gear ratios. For all cases the link inertia and desired inertia are constant at $J_D = 5J_G$. At $N=100$, $J_T = 10J_G$. At the lowest gear ratio ($N=10$), J_D is actually greater than J_T (the relationship is shown in the legend). This is why at high frequencies, where the first term in (12) dominates, the low gear ratio is disadvantageous. Even in this case, a lower gear reduction saves energy at low frequencies. At $N=50$, J_D is very close to J_T, but slightly smaller. Therefore, the inertia term does not dominate until very high frequencies. The other ratios are much more typical, in that torque feedback is used to significantly reduce apparent impedance. In this case, the penalty for increasing N is significant. For example, increasing the gear ratio from 100 to 200 increases the average total power by ~2x or more across all frequencies.

The following examples follow a similar process. Damping is often omitted from the equations for brevity.

Pure Torque Control Another widely-used case is pure torque control, wherein the desired impedance is zero and the output torque is entirely independent of motion. Because all dynamics must be suppressed, this can be approximated with $\tau_O=0$, or $J_D=0$ in (11). The zero torque case is itself of particular interest, e.g. for exoskeletal and rehabilitation devices which seek to avoid loading the subject within certain parameters. If damping is omitted (for brevity), the power reduces to:

$$P_M = \left[\frac{(N^2 J_M + J_G)}{K_m N}\ddot{\theta}\right]^2 + \left[(N^2 J_M + J_G)\ddot{\theta}\right]\dot{\theta} \qquad (13)$$

Assumption of sinusoidal trajectories (as above) yields:

$$P_{avg} = \frac{1}{2}\left(\frac{N^2 J_M + J_G}{K_m N}\right)^2 \omega^4 \qquad (14)$$

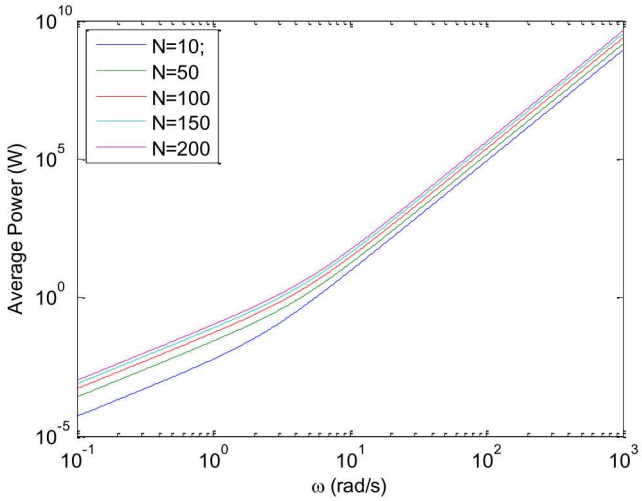

FIGURE 5. AVERAGE POWER VERSUS FREQUENCY FOR ZERO TARGET IMPEDANCE.

The power expended is a direct function of the physical impedance, and increases strongly with increases in N, (unless link inertia J_G dominates, which typically only occurs with very low N), as more and more control effort is expended to suppress the inertia. Thus, even if torque feedback produces the desired behavior, it can be extremely inefficient if the physical impedance is large. Figure 5 plots the expression in (14) for varying N.

Stiffness Control In a third case of interest, the closed-loop system is made to behave as a virtual spring at the point of interaction, following the relationship $\tau_O = K_D\theta$. Equation (7), with damping omitted, yields:

$$P_M = \left[\frac{(N^2 J_M + J_G)}{K_m N}\ddot{\theta} - \frac{K_D}{K_m N}\theta\right]^2 + \left[(N^2 J_M + J_G)\ddot{\theta} - K_D\theta\right]\dot{\theta} \qquad (15)$$

For cyclical trajectories,

$$P_{avg} = \frac{1}{2}\left[\frac{(N^2 J_M + J_G)}{K_m N}\omega^2 + \frac{K_D}{K_m N}\right]^2 \qquad (16)$$

This relationship is plotted in Fig. 6. The same parameters are used as for Fig. 4 and 5, with K_D=*100* Nm/rad. At frequencies below the break point (which is dictated by K_D and J_T), increased gearing provides strong energy benefits. At higher frequencies, increasing N requires more power.

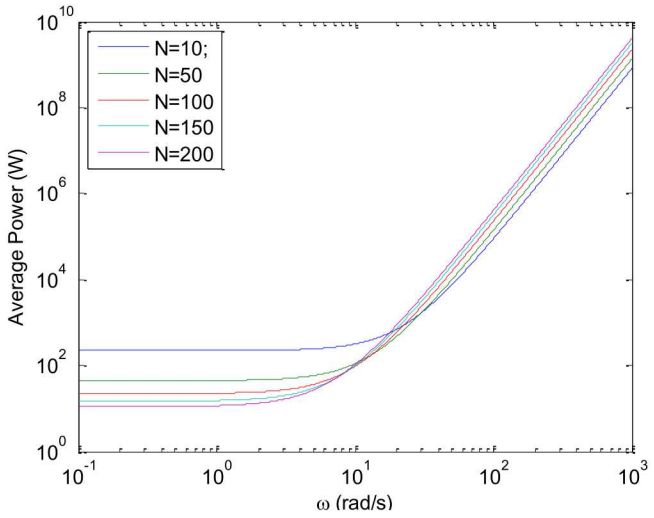

FIGURE 6. AVERAGE POWER VERSUS FREQUENCY FOR A VIRTUAL SPRING IN A TORQUE FEEDBACK MODEL.

ENERGY ANALYSIS OF SEA'S

For the reasons summarized in the introductory sections, a series elastic element is frequently added to torque feedback architectures. Here we examine the impact of this element on energy consumption.

Model

The model, shown in Fig. 7, resembles that of the previous section but includes a series spring with stiffness K_S coupling the gear output stage to an actuator output stage with position θ_O, moment of inertia J_O and damping coefficient B_O, to which τ_O is applied. The dynamics at the output are described by:

$$J_O\ddot{\theta}_O + B_O\dot{\theta}_O = \tau_O - K_S(\theta_O - \theta_G) \quad (17)$$

In most SEA designs, the mass and friction at the output stage are minimal compared to the robot links that they drive. To make the analysis easier to understand, J_O and B_O may be modeled as part of the load and neglected in the actuator model. This assumption does not substantively affect the results presented below, and produces:

$$\tau_O = K_S(\theta_O - \theta_G) \quad (18)$$

To analyze power consumption, the dynamics in terms of the output motions of the gearing are the same as in (1):

$$J_T\ddot{\theta}_G + B_T\dot{\theta}_G = N\tau_M + \tau_O \quad (19)$$

The ideal motor torque is the same as (3) in terms of θ_G:

$$\tau_M = \frac{J_T}{N}\ddot{\theta}_G + \frac{B_T}{N}\dot{\theta}_G - \frac{\tau_O}{N} \quad (20)$$

The motor power is the same as (6), but in terms of θ_G:

$$P_M = \left(\frac{J_T}{K_m N}\ddot{\theta}_G + \frac{B_T}{K_m N}\dot{\theta}_G - \frac{\tau_O}{K_m N}\right)^2 + \left(J_T\ddot{\theta}_G + B_T\dot{\theta}_G - \tau_O\right)\dot{\theta}_G \quad (21)$$

These equations are unchanged from the version without a spring; however the θ_G trajectories may vary from the actual output trajectories θ_O. In other words, any differences in energy consumption stem from the difference between the motion on the two ends of the spring. To compute power with respect to output behavior requires P_M in terms of θ_O. This is solved on a case-by-case basis below.

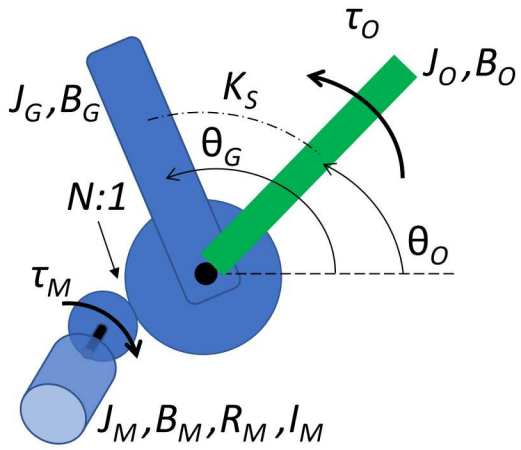

FIGURE 7. MODEL OF ROTARY SERIES ELASTIC ACTUATOR.

Control Cases of Interest

For these cases, we maintain fixed N and consider the motor and link inertias as one, for clarity.

Inertial Control A relationship generating inertial dynamics is:

$$\tau_O = J_D\ddot{\theta}_O = K_S(\theta_O - \theta_G) \quad (22)$$

To relate θ_G to θ_O, we take the Laplace transform and solve, where σ is the Laplace variable:

$$\theta_G = \theta_O\left(1 - \frac{J_D\sigma^2}{K_S}\right) \quad (23)$$

Substituting in (21) and returning to the time domain yields:

$$P_M = \left[\frac{(J_T - J_D)}{K_m N}\ddot{\theta}_O - \frac{J_T J_D}{K_m N K_S}\theta_O^{(4)}\right]^2 + \left[(J_T - J_D)\ddot{\theta}_O - \frac{J_T J_D}{K_S}\theta_O^{(4)}\right]\left(\dot{\theta}_O - \frac{J_D}{K_S}\theta_O^{(3)}\right) \quad (24)$$

Analysis of cyclical trajectories yields:

$$P_{avg} = \frac{1}{2}\left(\frac{J_T J_D}{K_m N K_S}\omega^4 + \frac{(J_T - J_D)}{K_m N}\omega^2\right)^2 \quad (25)$$

The second term can be positive or negative depending on the relationship between the physical and target inertias. This expression is plotted in Fig. 8 for J_D less than, equal to, and more than J_T. In virtually all cases, softer springs cause significantly greater energy consumption, with the effect increasing with frequency. The only exceptions to this are narrow areas around particular frequencies for the case where the system is attempting to emulate a much greater inertia than the physical level (J_D>>J_T). For typical applications, SEAs and torque feedback are far more likely to be used to reduce, rather than increase, apparent inertia. This analysis suggests that to implement a broad, versatile capability to emulate various inertias, stiffer springs are more energy efficient.

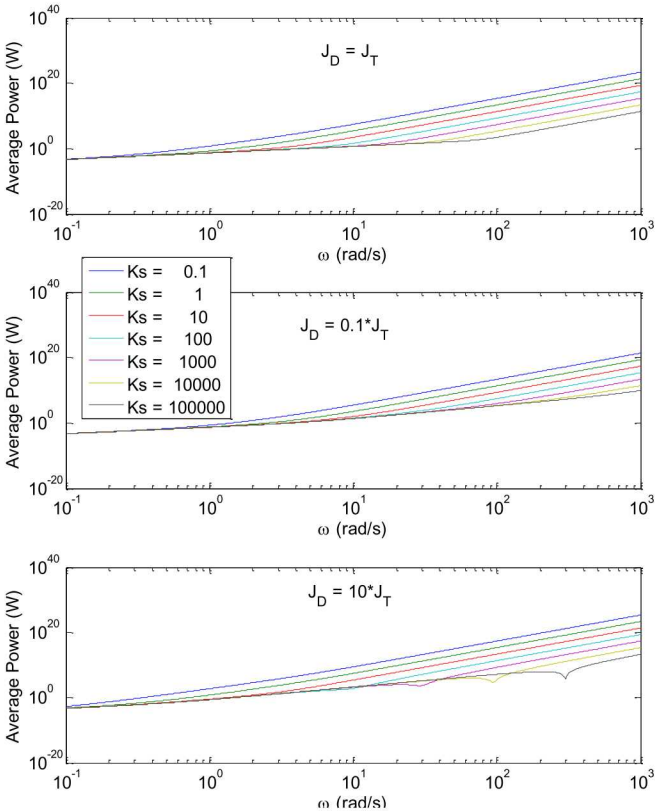

FIGURE 8. AVERAGE MOTOR POWER VERSUS FREQUENCY FOR SERIES ELASTIC ACTUATOR SYSTEM EMULATING VARIOUS DESIRED INERTIAS J_D.

Pure Torque Control For the case of pure torque control, $\tau_O = 0$ leads to $\theta_G = \theta_O$, from (19). Analytically, this is identical to the case with no spring, illustrated (with damping omitted) in (14) and Fig. 5; the spring does not affect energy consumption.

Stiffness Control Finally, stiffness control behavior is described by:

$$\tau_O = K_D\theta_O = K_S(\theta_O - \theta_G) \quad (26)$$

The resulting power relationship is:

$$P_M = \left(\frac{J_T(K_S - K_D)}{K_m N K_S}\ddot{\theta}_O - \frac{K_D}{K_m N}\theta_O\right)^2 + \left(\frac{J_T(K_S - K_D)}{K_S}\ddot{\theta}_O - K_D\theta_O\right)\left(\frac{K_S - K_D}{K_S}\right)\dot{\theta}_O \quad (27)$$

In the extreme, very small K_D converges to pure torque control and K_S has no effect. If K_D=K_S, all terms except the second drop out. In this isolated case, the physical spring provides the desired dynamics, and increasing N saves energy. However, this would clearly hinder efficient *versatile* functionality of the actuator.

For cyclic trajectories, the average power is:

$$P_{avg} = \frac{1}{2}\left(\frac{J_T(K_S - K_D)}{K_m N K_S}\omega^2 + \frac{K_D}{K_m N}\right)^2 \quad (28)$$

This is plotted in Fig. 9 for various values of K_S, with K_D=*100*. K_S=K_D provides an energy optimal condition, as noted above, at which power is independent of motion frequency. For K_S either smaller or larger, the power rapidly increases, particularly at higher frequencies. Physical stiffnesses below the desired value are particularly problematic, as these require the system to be driven beyond its inherent bandwidth. Stiffnesses greater than K_D provide some energy savings at high frequencies. However, savings are relatively modest, as indicated by the relatively small difference between K_S=*200* and K_S=*10000*, an effectively infinite value. These savings are dwarfed by the cost of trying to exceed the physical stiffness under any operating conditions. In practice, system designers will select a stiffness that is greater than any value they expect to emulate, and that will provide the bandwidth required for both nominal and recovery behaviors, with a healthy margin. This means that relatively stiff springs are typical.

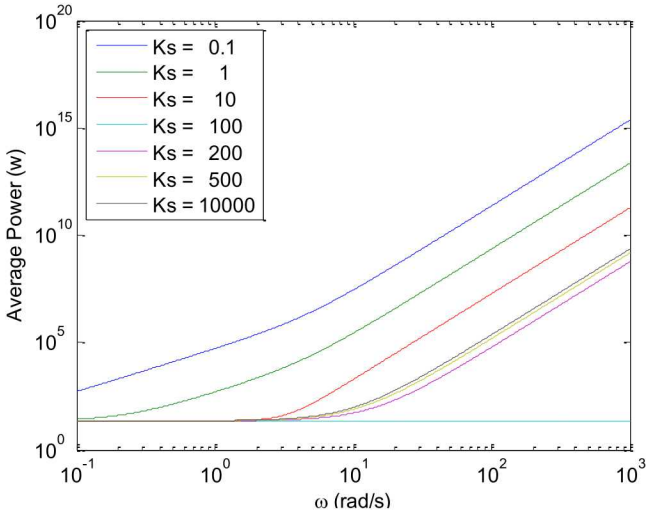

FIGURE 9. AVERAGE POWER VERSUS FREQUENCY FOR A SERIES ELASTIC ACTUATOR WITH A RANGE OF STIFFNESS VALUES. K_D=100.

LEGGED ROBOT SYSTEM DESIGN EXEMPLAR

The analysis in the preceding sections relies on simplified models of single joint drivetrains executing generalized cyclic trajectories. This elucidates, in a comprehensible form, overall energy consumption trends associated with using torque feedback control and SEAs to render various dynamic behaviors. The results are general and complete at a single-joint level, subject to the key assumptions: 1) motion is cyclic, 2) individual joint motion / torque trajectories are invariant with drivetrain design, 3) joint behaviors are idealized time-invariant inertias, springs, or motion-independent torque sources, 4) the model accurately reflects the drivetrain, and 5) motor parameters scale as described in (8). With these assumptions, the analytical results suggest that in many cases, choosing larger motors with small N is energetically preferable to smaller motors with large N, and that highly compliant SEAs offer little energetic benefit.

Drivetrain design for full robot systems involves greater complexity. In this section we present summary results of a comparative drivetrain design analysis for key leg joints on a pair of energy-efficient humanoid robots, the Sandia Transmission Efficient Prototype Promoting Research (STEPPR) and the Walking Anthropomorphic Novelly-Driven Efficient Robot for Emergency Response (WANDERER), shown in Fig. 1. These robots were designed to maximize endurance by minimizing their electrical energy consumption. While a detailed examination of the design of these robots is beyond the scope of this paper, summary results are examined to "sanity check" the overall conclusions of the single-joint analysis provided in the preceding sections in a more realistic system context.

The system-level design analysis differed from the single-joint analysis in the following three ways. First, a library of several different bipedal gait behaviors, including human walking (Human1 and Human2 gaits) and robot simulations (Humanlike, Crouched1 and Crouched2 gaits), was used to provide accurate representations of complex joint behaviors, which do not strictly equate to time-invariant inertias, springs, or motion-independent torque controls over all complete gait cycles. Second, models of three exemplar motors from the same family were used (Allied Motion MF0310025, MF0150025, and MF0095020), eliminating the need to make scaling assumptions. Finally, as motors were scaled the joint torque trajectories were scaled accordingly to appropriately penalize the use of larger motors. Torques were scaled in proportion to the ratio of: the robot mass with the selected motor set; to the robot mass in the baseline simulation. In STEPPR and WANDERER, (mass-dependent) gravity and inertial loads dominate all other loads due to the robots' extremely low-friction drivetrain [20].

For each topology and gait, numerical optimizations were conducted over the motion and torque trajectories to identify design parameters that minimized the total energy per gait cycle at each joint. First, as a baseline, the optimal N was determined for each choice of motor, for each gait, at each joint, assuming a topology as shown in Fig. 2. Predicted energetic costs per gait cycle, for each of the planar joints (ankle, knee, and hip) and each design gait, are shown in Fig. 10. Virtually all gait / joint pairs follow the overall trend: the intermediate ("Mid") motor requires the least energy. The smallest motor requires the most energy, and the largest motor requires an intermediate amount of energy that is close to the level required for the intermediate motor. As expected, the optimal gear ratios N scale inversely with the motor size. The average optimal gear ratio (mean +/- std. deviation) was 4.5 +/- 1.6 for the largest motor, 18.5 +/- 6.6 for the intermediate motor, and 43.3 +/- 15.0 for the smallest motor.

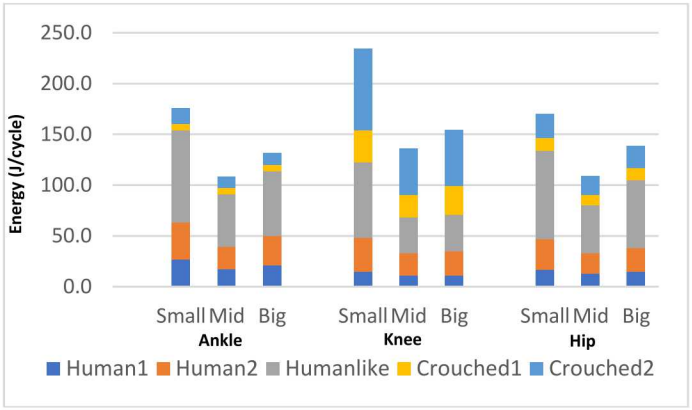

FIGURE 10. ENERGETIC COST PER GAIT CYCLE FOR EACH JOINT AND GAIT.

Subsequently, the topology of Fig. 7 was analyzed for each joint / gait pair by co-optimizing the stiffness K_S and gear ratio N. Figure 11 presents summary results in the form of percent savings, versus the baseline results from Fig. 10, provided by the introduction of series elasticity with the (best-performing) intermediate motor. Energy savings approach 10% in a few

cases, but are generally less than 4%, with 1/3 of the joint / gait pairs showing <0.1% savings. In these cases, the optimal K_S converges to the maximum value allowed by the analysis, 100kNm/rad, effectively eliminating the series elastic effect. For the cases where energy savings are realized, the optimal stiffness ranged from ~1000 to ~4000 Nm/rad. The other two motors had similar percentage energy savings with the addition of a series elastic element.

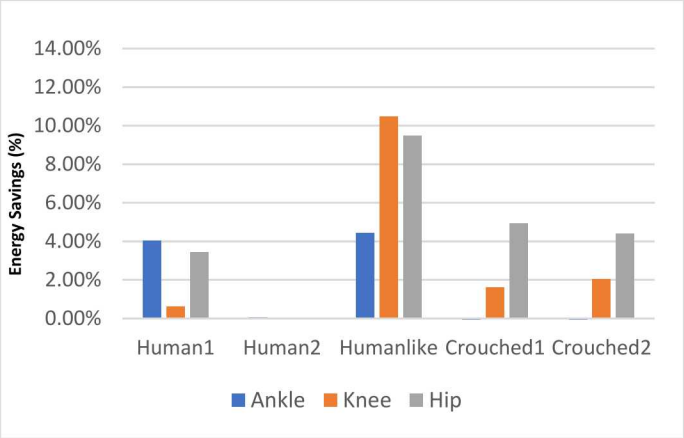

FIGURE 11. PERCENT ENERGY SAVINGS FROM OPTIMAL SERIES ELASTIC ELEMENT, RELATIVE TO BASELINE RESULTS IN FIG. 10.

Discussion

The results in Fig. 10 predict that in the absence of series elasticity, the intermediate sized motor, using gear reductions from ~8:1 to ~25:1, performs best. The smallest motor, paired with gear ratios of 30:1 or more, is more typical of many legged robot designs that use aggressive gearing to reduce motor mass. Our analysis predicts that for the robot architecture and gaits studied, such an architecture may be substantially less energy-efficient than using larger motors and less gearing – even when the increased joint torques caused by larger overall system mass, to support larger motors, is considered. Our analysis also predicts that using even larger motors with very modest gearing (<8:1) may require ~10-15% more energy than the intermediate motors, but still be much more efficient than highly-geared smaller motors. This is consistent with the results in Figs. 4 and 6, which show that very low gear ratios offer energetic benefits in some regimes (e.g. certain frequency ranges) and costs in others when the drive system emulates inertial or spring-like dynamic behavior. These regimes are defined by the relationship between the physical drivetrain dynamics and the target behavior, which is complex and time-variant for true legged trajectories. These results indicate that, at the very least, designers of robot drivetrains should consider the energy impact of larger-motor / lower-gear ratio architectures in the context of the specific dynamic behaviors required by their systems.

Results of the energy optimization of SEAs (Fig. 11) predict energy savings ranging from zero, with the elastic elements disappearing, to 10%, with joint stiffness values in the 1000-4000 Nm/rad range. To place these joint stiffness and energy savings numbers into context, the results may be compared to those predicted for the alternative architecture of parallel elasticity, which is discussed in detail elsewhere [21]. When optimized, joints that use springs placed in *parallel* (rather than series) with geared motors, applied to same gaits, behaviors, and motor models, predict energy savings ranging from 6% to 53%. These results are introduced only to clarify that the 0-10% energy savings predicted using SEAs are much smaller than the maximum possible using passive dynamic elements. As predicted, SEAs provide comparatively little energy benefit.

Optimal parallel spring stiffness values for these gaits and joints are all less than 300 Nm/rad, which provides some indication of characteristic joint behavior. The energy-optimal SEAs use stiffness values approximately an order of magnitude greater; this stems from the need to maintain drive stiffness well above that of typical joint behavior to provide sufficient bandwidth for high-frequency components of real-world gait behaviors without suffering the severe energy penalties at high frequencies predicted as shown in Figs. 8 and 9.

Ultimately, for the STEPPR and WANDERER robot designs, we chose drivetrains using large, high-torque motors and gear ratios of $N=10$ or less at each leg joint. These ratios were chosen for low energy consumption as well as to negate the need for torque sensing and feedback and the resulting complexity and stability risks; the robots achieve torque control via current control. Ultimate robot results were quite promising, with the fully self-powered 93 kg WANDERER robot able to walk continuously using less than 300 W of total locomotive power.

CONCLUSIONS

This paper presents analyses of the energy implications of impedance and torque control drivetrain architectures that use significant gearing and/or series elastic elements to help render apparent impedance that differs significantly from that of the physical system. These architectures are widely used, generally with the goal of achieving quality impedance control performance using small, lightweight actuators. As they become more prevalent, it is important to consider the impact of these design topologies on energy consumption.

Our energy-focused analysis indicates that in many cases, high gear ratios cause substantial energy losses – particularly in cases where the gear ratios move the intrinsic impedance away from target behaviors. Large gear ratios produce large reflections of motor inertia and damping to the output; if low impedance is desired, the actuator must actively suppress these dynamics, which costs energy. In particular, when pure torque control (zero impedance) is desired, increasing the gear ratio is quite detrimental. In contrast, there are some cases in which increased gearing saves substantial energy – generally when high

impedance behavior is desired, and for low-frequency spring-like behavior.

Similarly, our analysis finds that series elasticity does not significantly improve the energy picture for such systems. For many cases, the stiffest springs are most energy-efficient, while for other cases the series springs offer some net energy benefit but gains are relatively modest. Of course, series springs offer other potential benefits which may outweigh potential energy expenditures for certain applications.

This work provides a framework for evaluating the energy impact of torque feedback and series elastic topologies in physically interactive robots. As increasingly functional capabilities are demonstrated in fields such as legged robots, mobile manipulators, and exoskeletons, we anticipate that energy efficiency will become a more prevalent concern, making analysis like this more important.

ACKNOWLEDGMENTS

This work was funded in part by the DARPA Maximum Mobility and Manipulation Program.

Sandia National Laboratories is a multimission laboratory managed and operated by National Technology & Engineering Solutions of Sandia, LLC, a wholly owned subsidiary of Honeywell International Inc., for the U.S. Department of Energy's National Nuclear Security Administration under contract DE-NA0003525. This paper describes objective technical results and analysis. Any subjective views or opinions that might be expressed in the paper do not necessarily represent the views of the U.S. Department of Energy or the United States Government.

REFERENCES

[1] L. Villani and J. De Schutter, "Force control," in *Springer handbook of robotics*, B. Siciliano and O. Khatib, Eds. Springer, 2016, p. 195.

[2] N. Hogan and S. P. Buerger, "Impedance and interaction control," in *Robotics and automation handbook*, T. Kurfess, Ed., CRC, 2005, 19.

[3] G.A. Pratt and M.M. Williamson, "Series elastic actuators," in *Proc. Int. Conf. Intelligent Robots and Systems*, 1995.

[4] K. Kong *et al.*, "Control of rotary series elastic actuator for ideal force-mode actuation in human–robot interaction applications," *IEEE/ASME Trans. Mechatron,* vol 14, pp. 105-118, 2009.

[5] A. Edsinger-Gonzales and J. Weber. "Domo: A force sensing humanoid robot for manipulation research." In *Proc. Int. Conf. Humanoid Robots,* 2004.

[6] J.F. Veneman *et al.,* "A series elastic-and bowden-cable-based actuation system for use as torque actuator in exoskeleton-type robots." *Int. J. Robotics Research*, vol. 25, no. 3, pp. 261-281, 2006.

[7] S. Yi *et al.*, "Team THOR's Entry in the DARPA Robotics Challenge Trial 2013," *J. Field Robotics,* vol. 32, no. 3, pp. 315-335, 2015.

[8] J. Pratt *et al.*, "Capturability-based analysis and control of legged locomotion, Part 2: Application to M2V2, a lower body humanoid," *Int. J. Robotics Research,* vol. 31, no. 10, pp. 1117-1133, 2012.

[9] N. Paine *et al.*, "Actuator Control for the NASA-JSC Valkyrie Humanoid Robot: A Decoupled Dynamics Approach to Torque Control of Series Elastic Robots," *J. Field Robotics,* vol. 32, no. 3, pp. 378-396, 2015.

[10] J.E. Colgate and N. Hogan. "Robust control of dynamically interacting systems," *Int. J. Control,* vol. 48, no. 1, pp. 65-88, 1988.

[11] W.S. Newman, "Stability and performance limits of interaction controllers." *ASME J. Dynamic Systems Measurement Control,* vol. 114, p. 563, 1992.

[12] M. Dohring and W. Newman, "Admittance enhancement in force feedback of dynamic systems," in *Proc. IEEE Int. Conf. Robotics and Automation,* vol. 1, 2002.

[13] P. Beckerle *et al.*, "Series and Parallel Elastic Actuation: Influence and Operating Positions on Design and Control,"*IEEE/ASME Trans. Mechatron.*, vol. 22, no. 1, pp. 521-528, 2017.

[14] T. Verstraten *et al.*, "Series and Parallel Elastic Actuation: Impact of natural dynamics on power and energy consumption," *Mechanism and Machine Theory*, vol. 102, pp. 232-246, 2016.

[15] Y. Yesilevskiy *et al.*, "A Comparison of Series and Parallel Elasticity in a Monopod Hopper," *Proc. IEEE Int. Conf. Robotics and Automation,* pp. 1036-1041, 2015.

[16] T. Verstraten *et al.*, "Optimizing the Power and Energy Consumption of Powered Prosthetic Ankles with Series and Parallel Elasticity," *Mechanism and Machine Theory*, vol. 116, pp. 419-432, 2017.

[17] J. Jasmin *et al.*, "Comparison of elastic configurations for energy efficient legged locomotion," *Proc. Australian Conf. Robotics and Automation,* pp. 1-8, 2015.

[18] T. Verstraten *et al.*, "Energy Consumption of Geared DC Motors in Dynamic Applications: Comparing Modeling Approaches," *IEEE Robotics and Automation Lett.*, vol. 1, no. 1, pp. 524-530, 2016.

[19] S. Rezazadeh and J. Hurst, "On the Selection of Motors and Transmissions for Electromechanical and Robotic Systems," *Proc. Int. Conf. Intelligent Robots and Systems,* 2014, pp. 4605-11, 2014.

[20] A. Mazumdar et al., "Synthetic fiber capstan drives for highly efficient, torque controlled, robotic applications." *IEEE Robotics Autom. Letters,* vol. 2, no. 2, pp. 554-561, 2017.

[21] A. Mazumdar *et al.*, "Parallel elastic elements improve energy efficiency on the STEPPR bipedal walking robot." *IEEE/ASME Trans. Mechatron.,* vol. 22, no. 2, pp. 898-908, 2017.

